

ELECTRON BEAM AT THE ADVANCED PHOTON SOURCE LINAC EXTENSION AREA BEAMLINE*

K. P. Wootton[†], W. J. Berg, M. Borland, A. Brill, J. M. Byrd, S. Chitra, J. Collins, J. C. Dooling, J. Edwards, L. Erwin, G. Fystro, T. Grabinski, M. Henry, E. Heyeck, J. Hoyt, R. Keane, S.-H. Lee, J. Lenner, I. Lobach, A. H. Lumpkin, A. Puttkammer, V. Sajaev, N. S. Sereno, Y. Sun, J. Wang, S. G. Wang, A. A. Zholents, Argonne National Laboratory, Lemont, IL, USA

Abstract

The Linac Extension Area has been developed into a beamline area for testing accelerator components and techniques. Beginning commissioning activities in February 2023, we have delivered the first electron beam to the Linac Extension Area at the Advanced Photon Source at 425 MeV. In the present work, we outline the stages of re-commissioning the electron beamline. We summarise measurements of the electron beam transport through the accelerator. We outline scenarios used to verify the adequacy of radiation shielding of the beamline, and measured shielding performance.

INTRODUCTION

The Linac Extension Area (LEA) at the Advanced Photon Source (APS) is a flexible beamline for accelerator component and technique development [1–4]. Hardware installation was completed in 2023, and activities to commission the electron beamline began in 2023.

In the present work, we summarise the progress to date in commissioning the LEA beamline. We outline the features of the LEA beamline. We summarise the stages of re-commissioning. We present measurements of the electron beam using beam diagnostics in the LEA enclosure during stages of commissioning. We outline the beam loss scenarios to be performed for qualifying the enclosure shielding.

LEA BEAMLINE

The LEA beamline lattice is configured to support ‘interleaving’ operation [5, 6]. Interleaving describes switching between a thermionic cathode radiofrequency electron gun (TCGun) as an electron source for APS storage ring operations, and a photocathode radiofrequency electron gun (PCGun) for LEA operations. We denote the LEA beamline as the section of beamline physically located within the LEA enclosure. The LEA beamline is illustrated in Fig. 1.

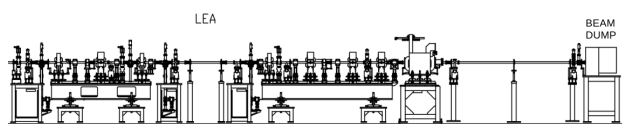


Figure 1: LEA beamline. In this figure the beam direction is from left to right.

As presently installed, the LEA beamline itself occupies ~15 m length within the LEA enclosure, terminating with an electron beam dump. A photograph of the LEA beamline is illustrated in Fig. 2.



Figure 2: Photograph of the LEA beamline within the LEA enclosure. In this figure the beam direction is from right to left.

The electron beam source for LEA is the APS linac. At present, the APS linac is capable of providing electron beams with energies up to ~450 MeV. The electron beam is transported from the APS linac to the LEA enclosure by several sections of beamline, denoted as the Particle Accumulator Ring bypass (PB), the PAR-to-Booster (PTB), and the Booster Bypass (BB) transport lines. The PAR bypass and PTB have been previously used for electron beam transport, and so for commissioning the LEA beamline, the main activity needed was to establish electron beam transport through the BB and LEA beamlines. The lattice of the booster bypass and LEA beamline for 425 MeV electrons is summarised in Table 1. The magnet types XX:QX correspond to upright quadrupoles, and XX:BX to skew dipoles (vertically deflecting). Numerous horizontal and vertical correctors are also included in the beamlines, but omitted from Table 1 for readability.

STAGES OF COMMISSIONING

The principal consideration in commissioning with the electron beam is that the LEA beamline is located within the LEA enclosure. This enclosure had previously been used for the Low-Energy Undulator Test Line (LEUTL) [7–9], but it

* Work supported by the U.S. Department of Energy, Office of Science, Office of Basic Energy Sciences, under Contract No. DE-AC02-06CH11357.

[†] kwootton@anl.gov

Table 1: Booster Bypass, Alcove and LEA Lattice

| Element | Position s (m) | Length l (m) | Gradient |
|-----------|---------------------|-------------------|-------------------------|
| BB:QE1 | 20.872 | 0.153 | 4.75 T m ⁻¹ |
| BB:QE2 | 21.399 | 0.153 | -5.95 T m ⁻¹ |
| BB:Q1 | 21.989 | 0.153 | 2.55 T m ⁻¹ |
| BB:BM:1-1 | 22.383 | 0.110 | -9.36 mrad |
| BB:BM:1-2 | 22.553 | 0.110 | -9.36 mrad |
| BB:BM:1-3 | 22.723 | 0.110 | -9.36 mrad |
| BB:Q2 | 31.184 | 0.153 | -1.48 T m ⁻¹ |
| BB:Q3 | 40.379 | 0.153 | 0.93 T m ⁻¹ |
| BB:Q4 | 49.574 | 0.153 | -1.48 T m ⁻¹ |
| BB:BM:2-1 | 57.993 | 0.110 | 9.36 mrad |
| BB:BM:2-2 | 58.163 | 0.110 | 9.36 mrad |
| BB:BM:2-3 | 58.333 | 0.110 | 9.36 mrad |
| BB:Q5 | 58.769 | 0.153 | 2.83 T m ⁻¹ |
| BB:Q6 | 60.642 | 0.153 | -5.17 T m ⁻¹ |
| LA:Q1 | 68.045 | 0.153 | 3.05 T m ⁻¹ |
| LA:Q2 | 69.198 | 0.153 | 4.21 T m ⁻¹ |
| LEA:Q1 | 74.186 | 0.100 | 8.72 T m ⁻¹ |
| LEA:Q2 | 75.190 | 0.153 | -7.61 T m ⁻¹ |
| LEA:Q3 | 76.112 | 0.100 | 3.90 T m ⁻¹ |
| LEA:Q4 | 79.053 | 0.100 | 9.07 T m ⁻¹ |
| LEA:Q5 | 80.004 | 0.153 | -7.16 T m ⁻¹ |
| LEA:Q6 | 81.004 | 0.153 | 7.31 T m ⁻¹ |
| LEA:Q7 | 81.666 | 0.153 | -5.79 T m ⁻¹ |
| LEA:BD | 82.274 | 0.500 | 200 mrad |

has been several years since beam was introduced to the enclosure [10]. This motivated the need for a readiness review prior to commissioning the beamline in a staged approach. Commissioning activities performed are broken into two stages: transport to the BB dump, and transport to the LEA beamline. The electron source used for these commissioning tasks was TCGun rather than the nominal PCGun. TCGun is capable of generating the greatest electron beam current and as such represents the principal radiological risk needing experimental validation.

Beam Transport to BB Dump

The BB dump is essentially located at the start of the BB transport line. This allows us to tune up beam transport through the upstream PB and PTB transport lines. Beam transport to the BB dump was established using diagnostics along the beam transport line. The principal diagnostics used in these studies were beam position monitors and beam profile monitors. The principal optimisation needed to establish beam through to the BB dump was transverse steering using corrector magnets.

Beam Transport to LEA

Transporting beam to LEA requires transporting beam through the BB and LEA beamlines. The booster bypass beamline is a vertical chicane rising in elevation by ~1 m over a length of ~40 m. Focussing quadrupoles are included

within the lattice. We began beam transport by tuning the vertical bending magnets to optimise electron transport at a beam energy of 425 MeV.

BEAM MEASUREMENTS

The principal diagnostics used for this study included area radiation monitors, handheld portable radiation monitors, electron beam position monitors, beam profile monitors and beam current monitors.

The first signature of electron transport to LEA was observed using area radiation monitors. An area radiation monitor is positioned within the LEA enclosure. This was the first indication that electrons had been successfully transported. Signals were subsequently quickly observed on the beam current monitors and beam position monitors (BPMs) in the LEA enclosure. Signals on the first electron beam position monitor within the LEA enclosure are illustrated in Fig. 3.

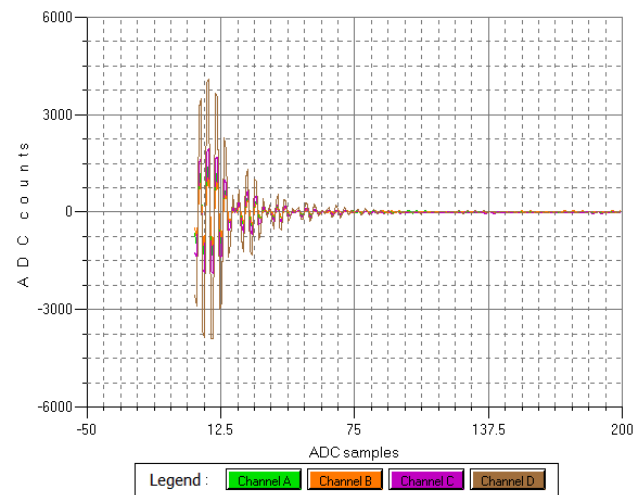


Figure 3: First observation of electron beam in the LEA enclosure measured using signals on the electron BPM.

The electron beam position was observed along the BB and LEA beamlines using all the BPMs in both transport lines. This is illustrated in Fig. 4.

With beam transported through to LEA, we were able to begin tuning up and focussing the electron beam using the beam profile monitor immediately adjacent to the electron beam dump. The visible area of the Cerium-doped Yttrium Aluminium Garnet (Ce:YAG) scintillator is 16 mm diameter. This is illustrated in Fig. 5.

BEAM LOSS SCENARIOS

A critical step in commissioning is validation of the shielding performance. At the APS, the shielding is experimentally validated using beam loss scenarios. Loss scenarios were meant to assess the radiation levels in and around the LEA enclosure under ‘normal’ and ‘off-normal’ beam conditions. It was not our intention to evaluate losses in previously commissioned transport beamlines upstream of LEA (PB, PTB, BB).

Content from this work may be used under the terms of the CC-BY-4.0 licence © 2023. Any distribution of this work must maintain attribution to the author(s), title of the work, publisher, and DOI

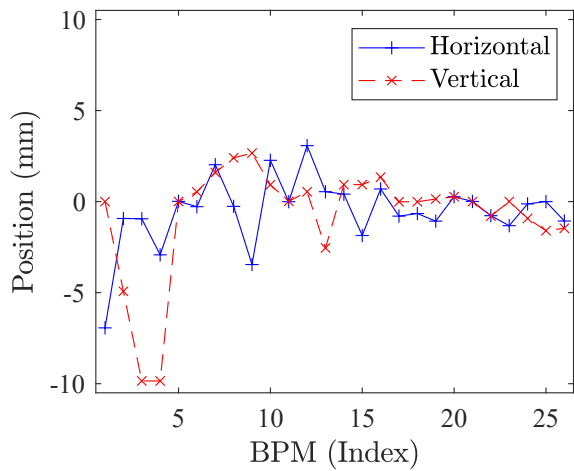


Figure 4: Beam observed using BPMs along booster bypass and LEA. In this figure, the beam trajectory is from left to right. Horizontal and vertical BPM signals are displayed. The horizontal plot axis is BPM index: the BPMs are not equally spaced along the beamline. BPMs 23-26 are the four BPMs in the LEA section of the beamline.

The loss scenarios considered included:

1. No acceleration of beam in the linac (background)
2. Beam to the LEA beam dump (nominal operations)
3. Beam strike on gate valve (GV) 1, GV1.
4. Beam strike on GV3.
5. Steering beam vertically upwards with corrector magnets.
6. Steering beam vertically downwards with corrector magnets.
7. Steering beam horizontally left with corrector magnets.
8. Steering beam horizontally right with corrector magnets.
9. Steering beam vertically upwards with corrector and quadrupole magnets.
10. Steering beam horizontally left with corrector and quadrupole magnets.
11. Steering low-energy beam vertically upwards with corrector and quadrupole magnets.

In developing these scenarios, particular attention was paid to the possibility of oversteering a low energy beam [11]. In this case, the assumed deflection would arise from a large transverse offset of the electron beam from the centerline of multiple quadrupole magnets. The maximum potential angular excursion of an electron beam was determined using simulations in the code ELEGANT [12–14].

In simulation, we considered the possibility of transporting electrons with energy as low as 25 MeV to the LEA enclosure. Using 3D field maps of the quadrupole and corrector magnets, the maximum excursion angle of the electron

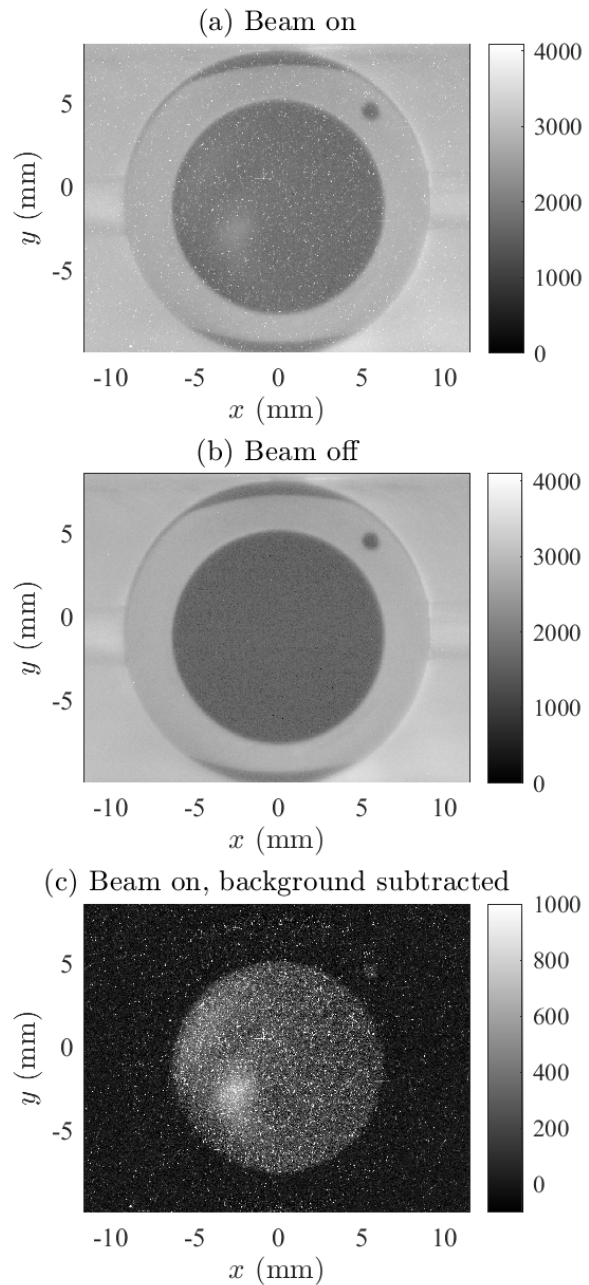


Figure 5: Observing electron beam at Ce:YAG LEA dump beam profile monitor. The top panel shows the image with the electron beam on, the middle panel shows an image with the electron beam off. The lower panel is the difference, showing the electron beam distribution.

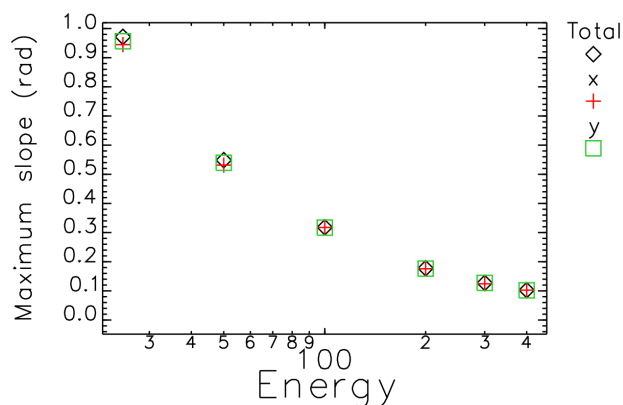


Figure 6: Calculated maximum excursion angle of electron beam at LEA [12].

beam at LEA was calculated over a range of electron beam energies 25–400 MeV. This is illustrated in Fig. 6.

Subsequently, we can use these excursion angles as input to radiological simulations. Radiological simulations of these loss scenarios were performed using MARS [15–18] and FLUKA [19, 20]. We consider several scenarios.

Normal operation of the electron beam transported to the electron beam dump is illustrated in Fig. 7. This simulation was performed assuming a 500 MeV electron beam energy, scaled to a maximum average electron beam current of 40 nA.

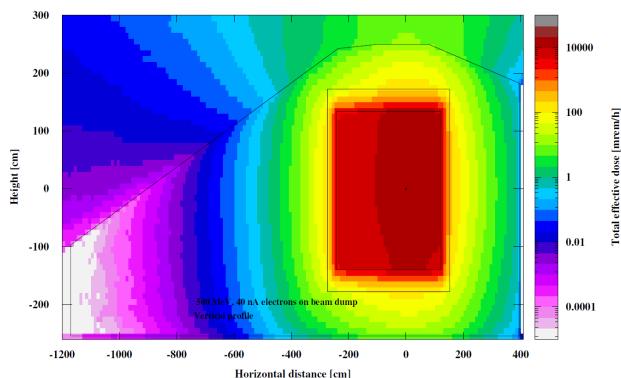


Figure 7: Radiological simulation of electron beam transport to the electron beam dump (Scenario 2) [21]. In this figure, the beam trajectory is into the page.

Maximum possible off-normal steering (vertical excursion) of the electron is illustrated in Fig. 8. This simulation was performed assuming a 300 MeV electron beam energy, scaled to a maximum average electron beam current of 40 nA.

These scenarios were developed to understand the safety consequences of proposed beam conditions. Of particular importance is that the normal operational electron beam current from the PCGun (average 2 nA) is much lower than simulated here for safety.

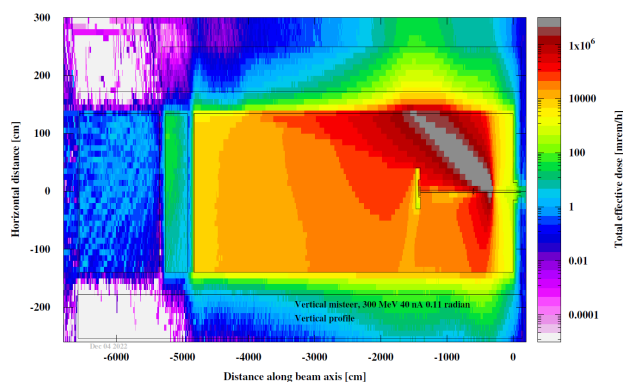


Figure 8: Radiological simulation of maximum possible off-normal electron beam vertical missteer (Scenario 9) [21]. In this figure, the beam trajectory is from right to left.

OUTLOOK

Due to schedule constraints, we were unable to complete measurement of the beam loss scenarios prior to the long shutdown of the APS accelerators to facilitate the start of installation of the Advanced Photon Source Upgrade (APS-U) storage ring. We hope to continue the commissioning process again at a future date.

SUMMARY

We have observed first electron beam to the LEA beamline at the APS. During commissioning activities, diagnostics including radiation monitors, beam position monitors, beam current monitors and beam profile monitors were usefully employed to detect and optimise the electron beam. We developed an extensive set of beam loss scenarios taking advantage of new simulation techniques, and incorporating lessons learned from previous commissioning activities. We began commissioning, but were unable to complete measurement of the beam loss scenarios prior to the long shutdown for APS-U installation.

ACKNOWLEDGEMENTS

We gratefully acknowledge the computing resources provided on Bebop, a high-performance computing cluster operated by the Laboratory Computing Resource Center at Argonne National Laboratory.

The submitted manuscript has been created by UChicago Argonne, LLC, Operator of Argonne National Laboratory (“Argonne”). Argonne, a U.S. Department of Energy Office of Science Laboratory, is operated under Contract No. DE-AC02-06CH11357. The U.S. Government retains for itself, and others acting on its behalf, a paid-up nonexclusive, irrevocable worldwide license in said article to reproduce, prepare derivative works, distribute copies to the public, and perform publicly and display publicly, by or on behalf of the Government. The Department of Energy will provide public access to these results of federally sponsored research in accordance with the DOE Public Access Plan. <http://energy.gov/downloads/doe-public-access-plan>

REFERENCES

- [1] Y. Sun *et al.*, “APS Linac Interleaving Operation”, in *Proc. IPAC’19*, Melbourne, Australia, May 2019, pp. 1161–1163. doi:10.18429/JACoW-IPAC2019-MOPTS119
- [2] W. Berg, J. C. Dooling, S. H. Lee, Y. Sun, and A. Zholents, “Development of the Linac Extension Area 450-MeV Electron Test Beam Line at the Advanced Photon Source”, in *Proc. IBIC’19*, Malmö, Sweden, Sep. 2019, pp. 219–221. doi:10.18429/JACoW-IBIC2019-MOPP048
- [3] K. P. Wootton *et al.*, “The Advanced Photon Source Linac Extension Area Beamline”, in *Proc. NAPAC’22*, Albuquerque, NM, USA, Aug. 2022, pp. 430–432. doi:10.18429/JACoW-NAPAC2022-TUPA36
- [4] E. A. Nanni *et al.*, “C³ Demonstration Research and Development Plan”, SLAC National Accelerator Laboratory, Menlo Park, CA, USA, Rep. SLAC-PUB-17660, Jul. 2022. doi:10.48550/arXiv.2203.09076
- [5] S. Shin, Y. Sun, and A. Zholents, “Interleaving Lattice Design for APS Linac”, in *Proc. NAPAC’16*, Chicago, IL, USA, Oct. 2016, pp. 713–715. doi:10.18429/JACoW-NAPAC2016-WEPOA12
- [6] S. Shin, Y. Sun, J. Dooling, M. Borland, and A. Zholents, “Interleaving lattice for the Argonne Advanced Photon Source linac”, *Phys. Rev. Accel. Beams*, vol. 21, p. 060101, 2018. doi:10.1103/PhysRevAccelBeams.21.060101
- [7] M. White *et al.*, “Construction, Commissioning and Operational Experience of the Advanced Photon Source (APS) Linear Accelerator”, in *Proc. LINAC’96*, Geneva, Switzerland, Aug. 1996, paper TU301, pp. 315–319. doi:10.5170/CERN-1996-007.315
- [8] S. V. Milton, “Advanced Photon Source low-energy undulator test line”, in *Proc. SPIE 2988*, San Jose, CA, USA, May 1997, pp. 20–27. doi:10.1117/12.274387
- [9] S. V. Milton, J. N. Galayda, and E. Gluskin, “The Advanced Photon Source Low-Energy Undulator Test Line”, in *Proc. PAC’97*, Vancouver, Canada, May 1997, paper 3V021, pp. 877–879. <https://jacow.org/pac97/papers/pdf/3V021.PDF>
- [10] R. M. Lill *et al.*, “Design and Performance of the LCLS Cavity BPM System”, in *Proc. PAC’07*, Albuquerque, NM, USA, Jun. 2007, paper FRPMN111, pp. 4366–4368. <https://jacow.org/p07/papers/FRPMN111.pdf>
- [11] R. P. Filler *et al.*, “Results of NSLS-II Linac Commissioning”, in *Proc. IPAC’13*, Shanghai, China, May 2013, paper WEPWA083, pp. 2301–2303.
- [12] M. Borland, private communication, Dec. 2022.
- [13] M. Borland, “elegant: A flexible SDDS-compliant code for accelerator simulation”, Argonne National Laboratory, Lemont, IL, USA, Rep. Advanced Photon Source LS-287, Sep. 2000. doi:10.2172/761286
- [14] Y. Wang and M. Borland, “Implementation and Performance of Parallelized Elegant”, in *Proc. PAC’07*, Albuquerque, NM, USA, Jun. 2007, paper THPAN095, pp. 3444–3446. <https://jacow.org/p07/papers/THPAN095.pdf>
- [15] J. Dooling and A. A. Zholents, private communication, Jul. 2019.
- [16] N. V. Mokhov, “The Mars Code System User’s Guide Version 13(95)”, Fermilab, Batavia, IL, USA, Rep. Fermilab-FN-628, Feb. 1995.
- [17] N. V. Mokhov and S. I. Striganov, “MARS15 Overview”, *AIP Conf. Proc.*, vol. 896, pp. 50–60, Mar. 2007. doi:10.1063/1.2720456
- [18] N. V. Mokhov *et al.*, “MARS15 code developments driven by the intensity frontier needs”, *Prog. Nucl. Sci. Technol.*, vol. 4, pp. 496–501, 2014. doi:10.15669/pnst.4.496
- [19] C. Ahdida *et al.*, “New Capabilities of the FLUKA Multi-Purpose Code”, *Front. Phys.*, vol. 9, p. 788253, Jan. 2022. doi:10.3389/fphy.2021.788253
- [20] G. Battistoni *et al.*, “Overview of the FLUKA code”, *Ann. Nucl. Energy*, vol. 82, pp. 10–18, Aug. 2015. doi:10.1016/j.anucene.2014.11.007
- [21] S. Chitra, “Radiation Shielding Analysis of LEA”, unpublished.